



HAL
open science

Light Extraction and Brightness Enhancement of Luminescent Rectangular Slabs

P. Pichon, Lisa Lopez, Maxime Nourry-Martin, Stéphane Darbon, Frédéric Druon, Patrick Georges, François Balembois

► **To cite this version:**

P. Pichon, Lisa Lopez, Maxime Nourry-Martin, Stéphane Darbon, Frédéric Druon, et al.. Light Extraction and Brightness Enhancement of Luminescent Rectangular Slabs. *Advanced Photonics Research*, 2022, 3 (7), pp.2100356. 10.1002/adpr.202100356 . hal-03618185

HAL Id: hal-03618185

<https://hal.science/hal-03618185v1>

Submitted on 24 Mar 2022

HAL is a multi-disciplinary open access archive for the deposit and dissemination of scientific research documents, whether they are published or not. The documents may come from teaching and research institutions in France or abroad, or from public or private research centers.

L'archive ouverte pluridisciplinaire **HAL**, est destinée au dépôt et à la diffusion de documents scientifiques de niveau recherche, publiés ou non, émanant des établissements d'enseignement et de recherche français ou étrangers, des laboratoires publics ou privés.

Light Extraction and Brightness Enhancement of Luminescent Rectangular Slabs

Pierre Pichon,* Lisa Lopez, Maxime Nourry-Martin, Stéphane Darbon, Frederic Druon, Patrick Georges, and François Balembois


The extraction efficiency and the brightness are critical parameters to increase the performance of luminescent rectangular slabs such as scintillators, luminescent concentrators, or diamonds with NV centers. This work explains how an additional face breaking the rectangular symmetry can improve the extraction efficiency and brightness. The study is based on a fully analytical approach corroborated experimentally with cerium-doped yttrium aluminum garnet (Ce:YAG) slabs. The model gives an analytical expression of the extraction efficiency and the brightness of the additional face as a function of the slab parameters (dimensions, refractive index, losses). Results highlight that the extraction efficiency by an additional face can be improved even if the area of the additional face is lower than the area of the smallest face of the slab, generally chosen as the output face in a standard configuration. Therefore, the output brightness can be easily improved and controlled by the dimension of the additional face. Balancing the extraction efficiency and the brightness, a $1 \times 3 \times 22 \text{ mm}^3$ Ce:YAG slab with an optimized edge face and with mirrors on the lateral faces exhibits an efficiency 1.9 times better and a brightness 5.6 higher than a Ce:YAG in a standard configuration.

1. Introduction

Materials emitting incoherent light isotropically are used in various fields of applications such as lighting (blackbody radiation sources, light-emitting diodes (LEDs)), light-harvesting (luminescent solar concentrators), light conversion (scintillators), detectors for quantum measurement or magnetometry

P. Pichon, L. Lopez, M. Nourry-Martin, F. Druon, P. Georges, F. Balembois
Université Paris-Saclay
Institut d'Optique Graduate School
CNRS
Laboratoire Charles Fabry
91127 Palaiseau, France
E-mail: pierre.pichon@institutoptique.fr

M. Nourry-Martin, S. Darbon
CEA, DAM, DIF
F-91297 Arpajon, France

 The ORCID identification number(s) for the author(s) of this article can be found under <https://doi.org/10.1002/adpr.202100356>.

© 2022 The Authors. Advanced Photonics Research published by Wiley-VCH GmbH. This is an open access article under the terms of the Creative Commons Attribution License, which permits use, distribution and reproduction in any medium, provided the original work is properly cited.

DOI: 10.1002/adpr.202100356

measurements (nitrogen-vacancies in diamonds). Because the light is emitted in a material having a refractive index larger than its surrounding (generally air), the transmission towards the output medium is limited by total internal reflection (TIR). The extraction efficiency, defined by the ratio of the light emitted by the useful exit face and the total light emitted inside the material, is therefore limited, especially for emitting media with high refractive indices. Optimizing the extraction efficiency has been extensively worked in the field of LEDs, leading to a complex structuration of the semiconductor output surface.^[1]

The isotropic emission leads to another limitation: the Lambertian-emission-related from the Fresnel reflections at the output interface corresponds to a solid angle often larger than the collection angle of the optical systems used for remote lighting or for detection applications, this limits the performance of the optical chain from

the source to the detector. Solutions have been carried out in LED with resonant cavities and metasurfaces,^[2] reducing the emitting solid angle and improving the brightness. Once again, this performance is enabled by semi-conductor engineering. This strategy may not be adapted for all isotropic sources, especially for massive homogeneous media like concentrators, scintillators, or NV diamonds. This is why light extraction has been explored for 70 years^[3–10] in the scintillator domain. However, it is also important to focus our attention on other media like luminescent concentrators^[11–26] and NV diamonds.^[27–32] The simplest and most common geometry reported is the rectangular slab (basically six parallel planes in pairs). Several strategies have been implemented to optimize the light extraction: the use of reflectors,^[8,33] the surface roughening,^[4,10,34] or the addition of extraction optics (which includes optical index adaptation).^[16,22,30–32,35–38] Some studies have investigated other geometrical configurations than rectangular slabs like hexagonal, cylindrical, pyramidal, triangular, and half-spherical shapes.^[7,8,39] However, those shapes tend to have a negative effect on the light guiding and can reduce the extraction efficiency compared to the simple rectangular slab. This explains why the most common shape used remains, after years of studies, the rectangular slab with an output surface chosen among the two smallest faces of the slab.

The purpose of this article is to show that simple geometric considerations such as an additional face can be successfully implemented to improve both light extraction and brightness of luminescent slabs. The article is structured as follows. Section 2 describes the role of the slab symmetries in the extraction efficiency through an additional face. Section 3 shows analytically that the output power and the brightness of the additional face can be controlled by its area, using the concept of light recycling.^[33,40] In Section 4, an experimental study with cerium-doped yttrium aluminum garnet (Ce:YAG) crystal is presented. Ce:YAG is a well-mastered industrial crystal with an emission spectrum peaking at the maximum human eye sensitivity. Hence, it has been used to develop many luminescent concentrators for lighting.^[16–21,33,34,40] This experimental study corroborates the analytical model and the performance of light extraction and brightness are analyzed versus different parameters of the slab (refractive index, size of the additional faces, and propagation losses).

2. The Interest of an Additional Face for Light Extraction

In 1990, Carrier and Lecomte studied experimentally the effect of a slanted output face in rectangular parallelepipedic bismuth germanate (BGO) scintillators^[9] and observed a higher output as soon as the face was tilted. This effect was attributed to the elimination of the symmetry of the slab, avoiding trapped rays in the structure. This effect was obtained when the other faces were covered by mirrors or by diffusing material like Teflon. More recently, a study by Gallinelli et al.^[34] on Ce:YAG slabs concluded to similar observations and results. Hence, the modification of the geometry of the luminescent rectangular slab seems to be an interesting way to extract trapped rays. However, modifying the angle of the output face increases its area. Therefore, a higher power can be extracted but the brightness does not necessarily increase.

Instead of modifying the geometry of the slab by tilting one of the six faces, we propose to add a tilted face with a small area, to generate a small perturbation of the rays propagating inside the rectangular slab. As opposed to previous investigations, where many tilt angles were investigated,^[9,34] the angle of the additional face was chosen with care to take benefit of the angular symmetry of the slab. The analysis proposed in this section considers that the propagation inside the medium is lossless.

2.1. Description of the Different Configurations

Let's consider a homogeneous luminescent medium shaped having a rectangular slab (6 flat faces parallels by pairs). The normal to the faces forms an orthonormal basis $(\vec{u}_x, \vec{u}_y, \vec{u}_z)$ as represented in **Figure 1a**. The slab is characterized by its length (l), width (w), and thickness (t). Three configurations corresponding to three different exit faces are investigated in this article (for the sake of simplicity, a face is referred to by its normal vector \vec{n}). 1) A standard output face corresponding to one of the smallest faces ($w \times t$) of the slab (**Figure 1b**). The face is orthogonal to the vector $\vec{n} (1,0,0)$. 2) An additional output face called “edge face” corresponding to a face orthogonal to the vector $\vec{n} (1,1,0)$

(**Figure 1c**). 3) An additional face called “corner face” corresponding to a face orthogonal to the vector $\vec{n} (1,1,1)$ (**Figure 1d**).

A light ray emitted inside the slab is characterized by a vector defined by cartesian coordinates (x, y, z) or by two angles (α and β in **Figure 1**). Fluorescence being isotropic, light is emitted inside the slab in 4π steradians and can be represented by a sphere (see the spheres in **Figure 1**). The rectangular slab has a refractive index n and is placed in air. The critical angle of total internal reflections (TIR) angle is defined by

$$\theta_{\text{TIR}} = a \sin\left(\frac{1}{n}\right) \quad (1)$$

The TIR condition defines a limit angle for a ray to escape by a given face. Therefore, each face has a specific escape cone of solid angle

$$\Omega_{\text{escape}} = 2\pi(1 - \cos\theta_{\text{TIR}}) \quad (2)$$

An escape cone is defined by a TIR angle and by its axis vector \vec{u} , which is also normal to the escape face. For the sake of simplicity, an escape cone is named only by its vector \vec{u} . Six escape cones $(1,0,0)$, $(-1,0,0)$, $(0,1,0)$, $(0,-1,0)$, $(0,0,1)$, $(0,0,-1)$, are related to the six faces of the slabs. These six cones intercept the sphere representing the 4π -steradian-emission in six spherical caps represented in green in **Figure 1**. The output cone is defined as the escape cone corresponding to the output face. The output face depends on the configuration investigated. In the standard configuration, the output cone is $\vec{u}=(1,0,0)$ (in blue in **Figure 1b**). When an additional face is added, a new output cone appears (blue cones on **Figure 1c,d**). Its coordinates are $\vec{u}=(1,1,0)$ in the case of the edge additional face and $\vec{u}=(1,1,1)$ in the case of the corner additional face.

2.2. Images of the Escape Cones by the Structure

In the first place, let us remind some basic principles about the evolution of the direction of light rays emitted inside a slab.^[3,34] The symmetries of the rectangular slab geometry generate great robustness of the ray direction conservation after reflection on the slab faces. For any ray inside the slab with a propagation direction defined by Cartesian coordinates (x, y, z) , a reflection on any face will flip the sign of the associated coordinates. Hence, the structure symmetries give only 8 possible directions: $(\pm x, \pm y, \pm z)$ corresponding to the red dots in **Figure 1b**: (four dots on the front cap and four dots on the back cap). This has two consequences: a ray belonging to one of the escape cones of the slab faces remains in its cone by reflection on the slab face and ends to leave the structure. On the opposite, a ray that does not belong to an escape cone is trapped forever in the structure (corresponding to the blue dots in **Figure 1b**). When an additional face is added, part of the trapped rays can be extracted (blue and red caps on **Figure 1c,d**) as already mentioned by previous investigations.^[9,34]

Let's consider now the images of the output cone through the structure assuming that the six planes of the slab are mirrors. In the standard configuration, since two coordinates are 0, the output cone whose axis is $(1,0,0)$ has only one image different from itself: $(-1,0,0)$ that is the cone in the opposite direction.

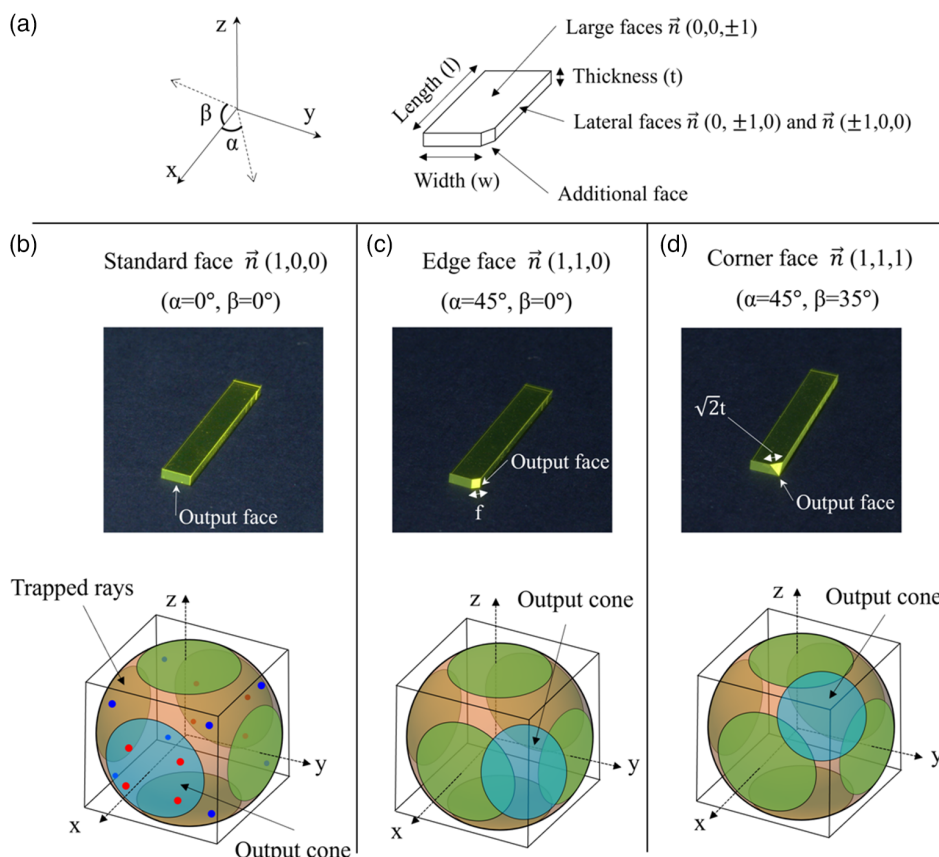


Figure 1. a) Definitions of the sizes and faces of a luminescent slab. Photographs and angular representations of the configurations studied in this article: b) standard-face configuration, c) edge-face configuration, and d) corner-face configuration. The output faces are defined by a normal vector \vec{n} . The three photographs of luminescent concentrators have been taken under the same pumping conditions and the same camera settings.

This means that all rays belonging to the cone $(-1,0,0)$ can be collected in the output cone $(1,0,0)$, providing that the face opposite to the output face is covered by a mirror (**Figure 2a**). This simple addendum is often used to increase the extraction efficiency.^[16–22] Experimentally, adding this mirror increases the

power emitted by the output face by a factor of 1.8 in the case of Ce:YAG. Therefore, we included a mirror in the standard configuration since it is quasi-systematically used in concrete cases.

In the case of the edge configuration, the output cone $(1,1,0)$ has three images $(-1,1,0)$, $(1,-1,0)$ and $(-1,-1,0)$ (**Figure 2b**).

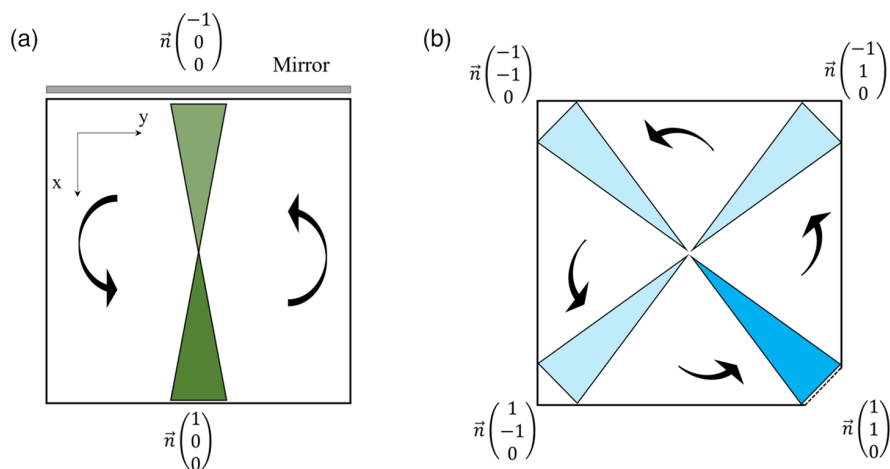


Figure 2. a) Connection of two spherical cones with a mirror in the standard face case. b) connection by the symmetry of four spherical cones in the case of the edge face. For readability, the figure is restricted in 2D for the (x,y) plane.

This means that the output cone can collect rays coming from three other cones, theoretically doubling the extraction efficiency, compared to a standard configuration with a mirror. In the case of the corner configuration, the output cone (1,1,1) has seven images ($\pm 1, \pm 1, \pm 1$). This means that the output cone can collect rays coming from seven other cones, potentially quadrupling the extraction efficiency, compared to a standard configuration with a mirror.

Despite its potential, the output by an additional face has limitations that are investigated in the following. The first limitation is the overlap between cones (Section 2.3). The second limitation comes from the perturbation induced by the additional face on the ray propagation (Section 2.4). The third limitation comes from the propagation losses in the structure (investigated in Section 3 and 4).

2.3. Overlap Between Escape and Output Cones

For a better understanding, let us consider planisphere representation in angles (α, β) (Figure 3). It shows how the output cone and its images may overlap the escape cones of the structure (rectangular slab). The standard configuration is less affected by cones overlap since the relative angle between cones is 90° (Figure 3a). The configurations with additional faces are more impacted because of a lower relative angle between cones: 45° in the edge configuration (Figure 3b) and 55° in the corner configuration (Figure 3c). Without mirrors on the six faces rectangular slab structure, the light extraction through the additional face will suffer from these overlaps: as the size of the additional face is assumed to be small compared to the other faces, a ray belonging to an escape cone of one of the six faces of the slab has much more chances to escape by one of its six regular faces than by the additional output face. Therefore, the overlap can be considered as loss.

To quantify the overlap, we define the overlapping ratio (η_{overlap}) as the portion of the output cone (or its images) common with the other escape cones of the structure. The overlapping ratio calculations are detailed in Section 6 and are, respectively, noted $\eta_{\text{overlap,s}}$, $\eta_{\text{overlap,e}}$, and $\eta_{\text{overlap,c}}$ for the standard, edge, and corner configuration. The overlapping ratio depends on the refractive index of the luminescent material (n). For values of n higher than 2.61, the escape cones are small and there is no overlap. The overlap appears for indices lower than 2.61 for the edge configuration, 2.16 for the corner configuration, and 1.41 for the standard configuration (Figure 4) in accordance with the immediate vicinity of the cones in the different configurations (Figure 3).

To avoid overlapping losses, the six faces of the rectangular slab could be covered by mirrors. It can be done in the case of scintillators, providing that the mirrors transmit high-energy particles. However, in case of optically pumped concentrators, like LED-pumped concentrators and even NV diamonds, the large faces ($w \times l$) are used to collect the pump light. Covering the lateral faces with mirrors remains a possible option. One mirror is added on the face opposite to the output face in the standard configuration studied in this work. Covering the four lateral faces is specifically studied in Section 4 for the edge configuration. In all the other cases presented in Section 2 and 3, no lateral mirrors are added for the edge and for the corner configuration.

2.4. Perturbation Induced by the Additional Face

The rays reaching the additional face \vec{n} are not necessarily in the output escape cone: indeed, a ray belonging to a cone with a vector \vec{u} such that $\vec{u} \cdot \vec{n} > 0$ can propagate up to the output face and be reflected by TIR.

In the edge configuration, with $\vec{n}(1, 1, 0)$, let's consider the cones that are coupled to the output cone: $(-1, -1, 0)$, $(-1, 1, 0)$, and $(1, -1, 0)$. The cone $(-1, -1, 0)$ has a negative scalar product $\vec{u} \cdot \vec{n}$, meaning that rays of this cone can not touch the output face. The cone axes $(-1, 1, 0)$ and $(1, -1, 0)$ have a scalar product $\vec{u} \cdot \vec{n} = 0$. This means that they are their own image by the additional face. Therefore, imaging by the additional face creates no perturbation in the edge configuration.

The corner configuration is different. Among the cones coupled to the output cone, three of them have a scalar product $\vec{u} \cdot \vec{n} > 0$: $(-1, 1, 1)$, $(1, -1, 1)$, and $(1, 1, -1)$. The images of those cones by the additional face can be calculated. For example, the cone $(1, -1, 1)$ is transformed to the cone $(\frac{1}{3}, -\frac{5}{3}, \frac{1}{3})$ by the additional face. This cone has a strong overlap with the $(0, -1, 0)$ escape cone corresponding to a lateral face. Therefore, rays belonging to this image will be lost through the lateral face. The same demonstration can be carried out for the other cones $(-1, 1, 1)$, and $(1, 1, -1)$. This means that a ray belonging to a cone coupled to the output cone may hit the output surface at the wrong angle (TIR) and may be reflected toward one of the six faces of the rectangular slab with the right angle to escape the structure. The emitted power lost by this process is denoted P_{lost} . The perturbation of the additional face can then be quantified by a factor η_d defined as

$$\eta_d = \frac{P_{\text{lost}}}{P_{\text{lost}} + P_{\text{out}}} \quad (3)$$

P_{out} being the output power through the additional face.

To evaluate η_d , let's consider what a ray "sees" inside the slab when it goes toward the output face. This can be visualized by unfolding the slab at each reflection on one of the six faces of the rectangular slab. The triangular corner face becomes a platonic octahedron (Figure 5a). The octahedron has an edge length of $\sqrt{2}t$ (t being the thickness of the slab). The area of a triangular face of the octahedron is $A_c = (\sqrt{3}/2)t^2$. When the octahedron is projected in the plane of the output face (Figure 5b), one can see three projections of the lateral faces of the octahedron. Those projections are seen by the cones $(-1, 1, 1)$, $(1, -1, 1)$, and $(1, 1, -1)$ when their rays hit the output surface. The central face (original corner face) is seen by the output cone $(1, 1, 1)$.

Let's define A_p , the area of the projection of one side triangle of the octahedron in the plane of the corner face. Since the dihedral angle of the octahedron is $\arccos(-1/\sqrt{3})$, The area of a lateral face projected is $A_p = t^2/(2\sqrt{3})$. A_p is equal to one-third of A_c . The reduction factor η_d is then

$$\eta_d = \frac{3A_p}{A_c + 3A_p} = 50\% \quad (4)$$

This means that the symmetry perturbation of the face reduces the output efficiency by 50%. This is balanced by the large number of cones coupled to the output face (8 for the

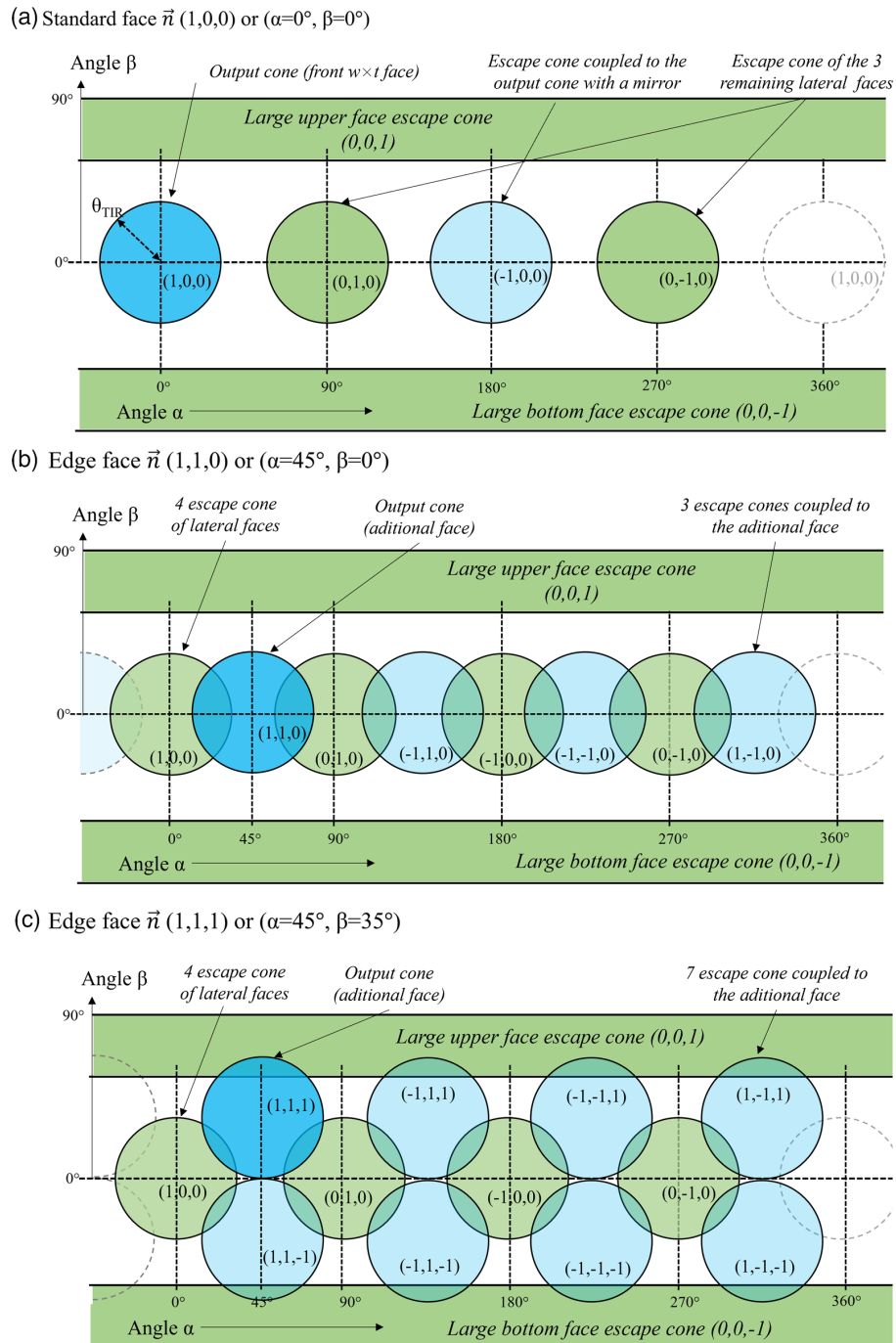


Figure 3. Planispheres representation of the angular representation in the case of cerium-doped yttrium aluminum garnet (Ce:YAG) ($n_{\text{YAG}} = 1.83$) in air showing the escape cones connections and overlaps for: a) the standard output face, b) the edge output face, and c) the corner output face. In this representation, for simplicity, the planisphere anamorphosis is only considered for the escape cones of the two large faces (north and south poles).

corner). Therefore, without additional mirrors, the edge configuration and the corner configuration should give similar results.

For further investigation, one must analyze the probability for a ray belonging to the output cone (and its images by the structure) to hit the additional face instead of the slab faces. This is carried out in the next part and will lead to the derivation of the power and the brightness of the output face.

3. Power and Brightness of Luminescent Rectangular Slabs

In the edge and corner configuration, the additional face is supposed to be small with respect to the other six faces of the rectangular slab. This means that rays belonging to the output escape cone have a strong probability of being reflected multiple

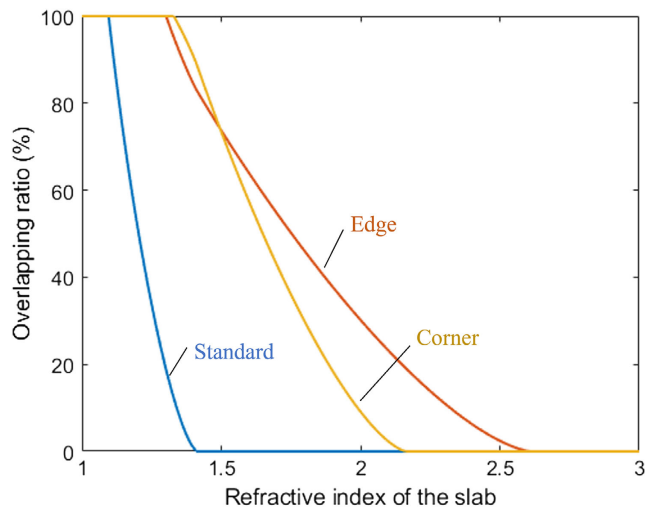


Figure 4. Overlapping ratio (overlap between escape and output cones) for the standard, edge, and corner configurations.

times in the structure before finding the output. This causes a recycling process of the light emitted inside the material. Obviously, light recycling increases the propagation length of a ray before it finds the exit. This will emphasize one of the limitations of the extraction by an additional face: the propagation losses in the structure, quantified by the loss coefficient α . One has to mention that light recycling in the standard case is also possible but with the help of adjustable mirrors as described in previous works.^[33,40] This case is not considered here.

This section is dedicated to the development of an analytical model describing the power, the light extraction, and the brightness of the exit face in the standard, edge, and corner configurations by taking into account a structure with propagation losses. It starts with the analysis of the standard output face.

3.1. Standard Case

The power emitted by one of a $w \times t$ face of a luminescent rectangular slab with a single opposite mirror of reflectivity R has been recently derived.^[33] The model considers that the slab contains luminophores with a uniform density per unit volume noted n_v , each of them emitting a power ϕ_e . The emitted power is

$$P_s = (1 - \eta_{\text{overlap},s}) \phi_e n_v w l t \frac{(1 - \cos \theta_{\text{TIR}})(1 + R e^{-\alpha d})(1 - e^{-\alpha d}) T}{2 \alpha d (1 - e^{-2 \alpha d} R (1 - T))} \quad (5)$$

with d the average propagation distance inside a rectangular slab of length l .

$$d = l \frac{\ln \cos(\theta_{\text{TIR}})}{\cos(\theta_{\text{TIR}}) - 1} \quad (6)$$

and T the Fresnel transmission defined by $T = 1 - \left(\frac{n-1}{n+1}\right)^2$.

The extraction efficiency corresponds to the ratio of the output power P_s to the total power emitted in the structure ($\phi_e n_v w l t$).

$$\frac{P_s}{\phi_e n_v w l t} = (1 - \eta_{\text{overlap},s}) \frac{(1 - \cos \theta_{\text{TIR}})(1 + R e^{-\alpha d})(1 - e^{-\alpha d}) T}{2 \alpha d (1 - e^{-2 \alpha d} R (1 - T))} \quad (7)$$

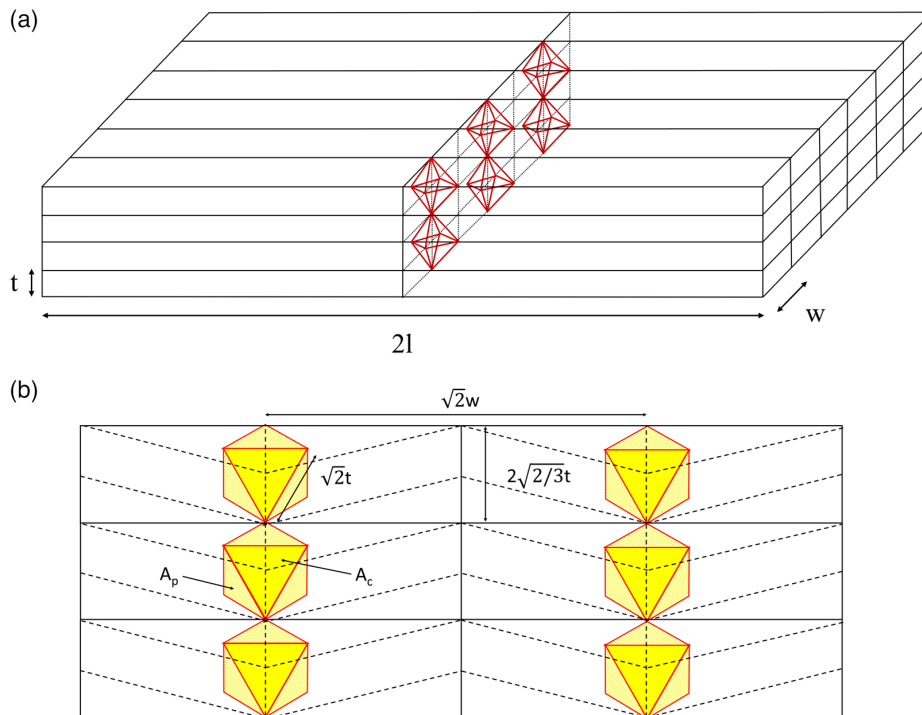


Figure 5. a) Unfolding of the rectangular slab with a corner face in all the directions of space. b) Projection in the plane of the output face.

As the output face of a luminescent concentrator is close to a Lambertian emitter, the brightness of the face is

$$B_s = \frac{P_s}{\pi w t} \quad (8)$$

3.2. Edge Face

The length of the additional face is noted f (Figure 1c). The power emitted by the edge face ($f \times t$) can be described analytically using the concept of light recycling.^[33,40] The principle of light recycling lies in the fact that the rays bounce several times by TIR inside the rectangular slab. Each time that the light encounters the plane of the output face, a portion of the rays escapes according to the probability $f/(\sqrt{2}w)$ (see the area ratio in Figure 6). The total emitted power is derived via the sum of the terms of a geometrical series with a common ratio of $f/\sqrt{2}w$ (corresponding to the light emitted each time that the plane of the exit face is crossed by rays). The average traveled distance between two chances to encounter the exit face is $2\sqrt{2}d$.

For better understanding, the calculation is described in detail in the following. The power related to the rays emitted in the (1,1,0) and (1,-1,0) escape caps is

$$P_{(1,1,0)} = P_{(1,-1,0)} = \frac{\phi_e n_1 w l t}{2\sqrt{2} \alpha d} (1 - \cos \theta_{RTI}) (1 - e^{-\sqrt{2} \alpha d}) \quad (9)$$

The power incident on the exit face related to the first time that light crosses the plane of the exit face is

$$P_{(1,1,0),1} = \frac{f T}{\sqrt{2} w} P_{(1,1,0)} \quad (10)$$

A part of the light did not encounter the exit face and is recycled inside the rectangular slab and propagates an average distance of $2\sqrt{2}d$ before having another chance to be extracted. The output power after the second time that light crosses the plane of the exit face is

$$P_{(1,1,0),2} = \frac{f T}{\sqrt{2} w} e^{-2\sqrt{2} \alpha d} \left(1 - \frac{f T}{\sqrt{2} w}\right) P_{(1,1,0)} \quad (11)$$

The total output power from this escape cap is

$$P_{(1,1,0),tot} = \sum_{k=0}^{\infty} P_{(1,1,0),k} = \frac{f T}{\sqrt{2} w} P_{(1,1,0)} \frac{1}{1 - e^{-2\sqrt{2} \alpha d} \left(1 - \frac{f T}{\sqrt{2} w}\right)} \quad (12)$$

The same method allows to find the contribution of the rays emitted in the (-1,1,0) and (-1,-1,0) escape caps with

$$P_{(-1,-1,0)} = P_{(-1,1,0)} = \frac{\phi_e n_1 w l t}{2\sqrt{2} \alpha d} (1 - \cos \theta_{RTI}) e^{-2\sqrt{2} \alpha d} (e^{\sqrt{2} \alpha d} - 1) \quad (13)$$

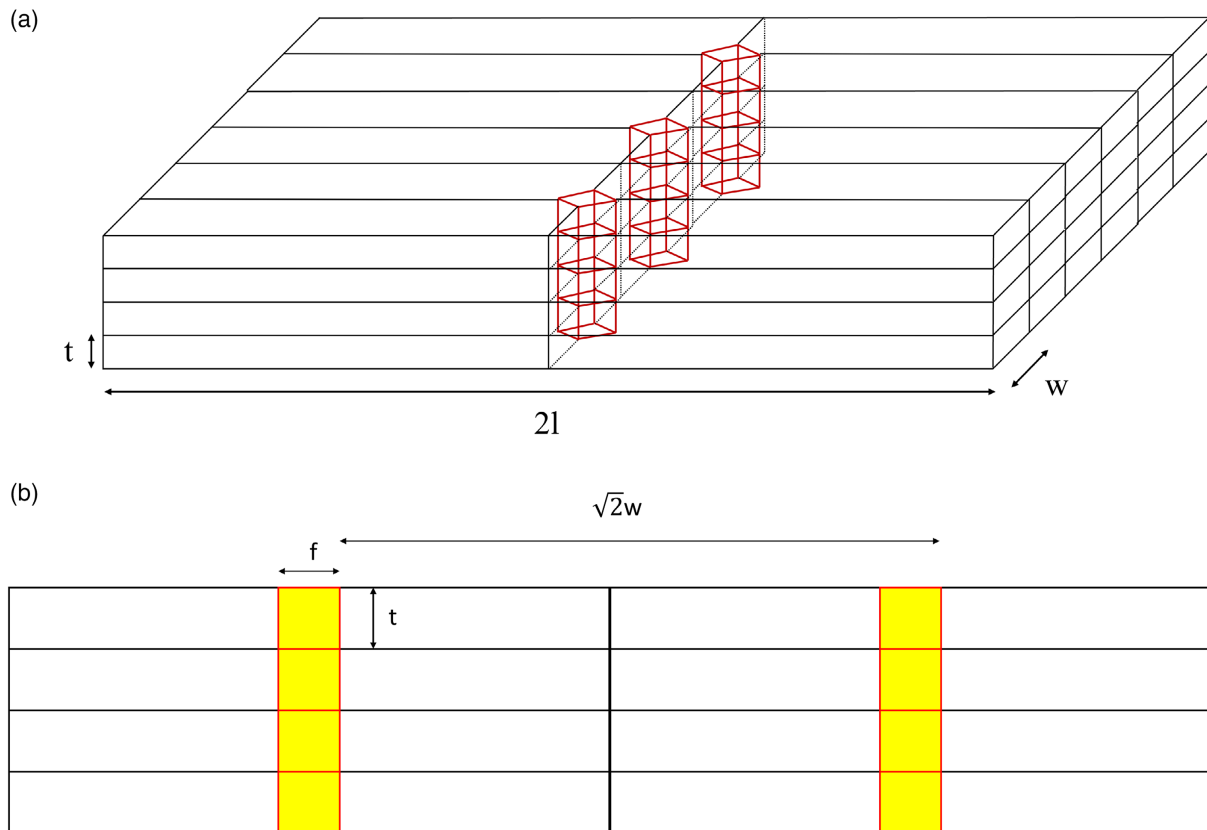


Figure 6. a) Unfolding of the rectangular slab with an edge face in all the directions of space. b) Projection in the plane of the output face.

By summing the contribution of each spherical cap and taking into account the overlapping ratio, the power emitted by the edge face is

$$P_e = (1 - \eta_{\text{overlap},e}) \sum P_{(\pm 1, \pm 1, 0), \text{tot}} \quad (14)$$

Equation (14) can be expressed literally by

$$P_e = (1 - \eta_{\text{overlap},e}) \frac{f}{w} \phi_e n_t w l t \frac{(1 - \cos \theta_{\text{RTI}})}{2\alpha d} \times \frac{(1 + e^{-\sqrt{2}\alpha d})(1 - e^{-\sqrt{2}\alpha d})T}{1 - e^{-2\sqrt{2}\alpha d}(1 - \frac{fT}{\sqrt{2}w})} \quad (15)$$

The extraction efficiency corresponds to the ratio of the output power P_e to the total power emitted in the structure, $\phi_e n_t w l t$

$$\frac{P_e}{\phi_e n_t w l t} = (1 - \eta_{\text{overlap},e}) \frac{f}{w} \frac{(1 - \cos \theta_{\text{RTI}})}{2\alpha d} \times \frac{(1 + e^{-\sqrt{2}\alpha d})(1 - e^{-\sqrt{2}\alpha d})T}{1 - e^{-2\sqrt{2}\alpha d}(1 - \frac{fT}{\sqrt{2}w})} \quad (16)$$

Assuming a Lambertian emission, the brightness of the edge face is

$$B_e = \frac{P_e}{\pi f t} \quad (17)$$

In the case of an edge face, the extraction efficiency can be optimized using mirrors on the four lateral faces of the slab. The derivation of the power emitted by the face when four mirrors are used is more tedious and requires a full development (see Supporting Information).

3.3. Corner Face

By analogy to the edge face case, the power extracted by the corner face can be described analytically with the help of the concept of light recycling.^[33] The traveled distance between two bounces in the plane of the escape face is now $2\sqrt{3}d$. In the case of a corner face, the probability for the light to be extracted each time it crosses the exit face plane is $3t/(8w)$. This corresponds to the ratio of the area of the corner face and the area of the projection of

the $w \times t$ face in the plane of the exit face (see the area ratio in Figure 5b). The power emitted by the corner face is

$$P_c = (1 - \eta_{\text{overlap},c})(1 - \eta_d) \frac{\sqrt{3} t}{2 w} \phi_e n_t w l t \frac{(1 - \cos \theta_{\text{RTI}})}{2\alpha d} \times \frac{(1 + e^{-\sqrt{3}\alpha d})(1 - e^{-\sqrt{3}\alpha d})T}{1 - e^{-2\sqrt{3}\alpha d}(1 - \frac{3tT}{8w})} \quad (18)$$

Similarly to the edge face, the overlapping ratio $\eta_{\text{overlap},c}$ has to be considered. But, contrary to the edge face case, some rays are deviated by the additional face and lost, corresponding to a reduction of power of $1 - \eta_d$, (Section 2.4).

The extraction efficiency corresponds to the ratio of the output power P_c to the total power emitted in the structure, $\phi_e n_t w l t$

$$\frac{P_c}{\phi_e n_t w l t} = (1 - \eta_{\text{overlap},c})(1 - \eta_d) \frac{\sqrt{3} t}{2 w} \frac{(1 - \cos \theta_{\text{RTI}})}{2\alpha d} \times \frac{(1 + e^{-\sqrt{3}\alpha d})(1 - e^{-\sqrt{3}\alpha d})T}{1 - e^{-2\sqrt{3}\alpha d}(1 - \frac{3tT}{8w})} \quad (19)$$

With A_c the area of the output face, the brightness of the additional corner face is then

$$B_c = \frac{P_c}{\pi A_c} \quad (20)$$

4. Analysis of the Analytical Model Compared to Experiments

The goal of this section is to explore the potential of the additional output face with the help of the analytical model. **Table 1** summarizes the main characteristics of the 3 configurations (standard face, edge face, and corner face) derived from Section 2 and 3. The table is completed by the average traveled distance^[40] for rays before reaching the output face. It is much longer in the case of the corner and edge configuration than the standard configuration which leads to a stronger influence of the propagation losses. As the propagation inside the slab can be important, we chose to test the interest of an additional face on a mature crystal grown in large dimensions: Ce:YAG.

Table 1. Comparison of the three configurations investigated in this article (standard, edge, and corner face).

	Standard face	Edge face	Corner face
Number of escape cones connected	2	4	8
Overlaps of the escape cone	for $n < 1.41$	for $n < 2.61$	for $n < 2.16$
Perturbation of rays (η_d)	–	–	50%
Area of the output face	$w t$	$f t$	$t^2 \sqrt{3}/2^a$
Average travelled distance ^{b)} (value ^{c)})	d (24 mm)	$(\frac{2\sqrt{2}w}{f} - 1)\sqrt{2}d$ (254 mm)	$(\frac{16w}{3t} - 1)\sqrt{3}d$ (623 mm)

^{a)}Area in the case of an equilateral triangle; ^{b)}The average travelled distance is calculated following the procedure described in the literature;^[40] ^{c)}For Ce:YAG in air with dimensions of the experiment.

4.1. Experimental Measurements with Ce:YAG Slabs

This section is dedicated to the experimental study and comparison with the analytical model.

The study was conducted on three single-crystal Ce:YAG slabs with dimensions $t = 1$ mm, $w = 3$ mm and $l = 22$ mm (pictures of Figure 1). The three dimensions of the slabs have an accuracy of ± 0.1 mm. The edge face was 1×1 mm² ($f = 1$ mm) and the corner face was an equilateral triangle with 1.4 mm sides (hence an area of 0.86 mm²). All the faces of the slabs were optically polished to scratch/dig 60/40. As a pump source, a blue laser diode emitting at 450 nm was used. The laser diode was placed 20 cm away from the slabs to produce a homogeneous pumping measured to be 2.2 mW cm⁻². The slabs were pumped on their largest faces ($w \times l$), on one side only (Figure 7). The transmission of the laser diode through the large face gave an absorption coefficient of 64 cm⁻¹ at 460 nm corresponding to a Ce³⁺ concentration of $n_t = 2.1 \times 10^{19}$ cm⁻³. Following the previous works on Ce:YAG, it is possible to estimate the mean propagation loss coefficient of the emission spectrum including passive losses due to scattering and self-absorption^[40] $\alpha = 3.8 \times 10^{-3}$ cm⁻¹ ($\alpha = 1.63 \times 10^{-22} \times n_t + 2.85 \times 10^{-4}$). Here α is an effective loss coefficient as self-absorption led to reemission in the wavelength region of interest.

The output light was collected by an integrating sphere placed in front of the output face. In each configuration, great care is taken to mask the light coming from the other faces. This setup allowed to make relative measurements of the power emitted by the face in different configurations. The value of reference corresponded to the performance of the output face in the standard configuration. From the measurements, extraction efficiency and brightness were deduced and compared to the theoretical curves presented in the following.

The measurements on the Ce:YAG slabs show that the extraction efficiency for the edge configuration is similar to the standard one. The corner face configuration allows to extract 21% more light than from the standard face. As the emitting area of the edge and corner faces are smaller than the standard face, it leads to much better brightness. 3.1 times and 4.2 times better for the edge configuration and for the corner configuration, respectively. The highest efficiency obtained in the corner configuration comes from the low overlap of the output cone and its images with the six escape cones of the rectangular slab structure (see Figure 3). Those performances confirm experimentally

the interest of an additional face. In the next subsections, the values are compared to the theoretical predictions.

4.2. Influence of the Surface of the Additional Face

Figure 8 shows the extraction efficiency and the brightness of the emitting face versus its area (normalized by the emitting area of the standard face ($w \times t$)). Experimental points were in good agreement with the theoretical curves within the accuracy of the measurements. The error bars were mainly given by the stability of the laser diode driver ($\pm 3\%$). Figure 8a shows that the extraction efficiency can be higher for edge and corner additional faces than for a standard output face (with mirror on the opposite). This was attributed to the number of cones coupled to the output. When the area of the emitting surface was reduced, the extraction efficiency fell. This is due to the larger average traveled distance increasing the losses for the rays before finding the output. However, thanks to light recycling and the low losses, the brightness increases when the emitting surface was reduced, with values several times higher than in the standard configuration. Therefore, it is possible to design edge and corner additional faces such that the extraction efficiency remains above the standard configuration, with a brightness significantly higher than standard faces: this has been done for the Ce:YAG samples tested in this study.

4.3. Influence of the Loss Coefficient

Figure 9 gives the influence of the loss coefficient α on the performance (extraction efficiency and brightness). It showed that edge and corner additional faces were interesting for light extraction only if the loss coefficient was sufficiently low: typically, below 5.10^{-3} cm⁻¹. This is the case in our experiment where $\alpha = 3.8.10^{-3}$ cm⁻¹. This coefficient corresponded to very low losses that cannot be found in every luminescent material for which well mastered crystal grown in large dimensions are therefore requested. In Figure 9, the curve related to the edge-face configuration decreased faster than those for the corner-face and for the standard-faces configuration. It indicated that the corner-face configuration was more sensitive to losses, since the average travel distance is higher in this configuration (see Table 1).

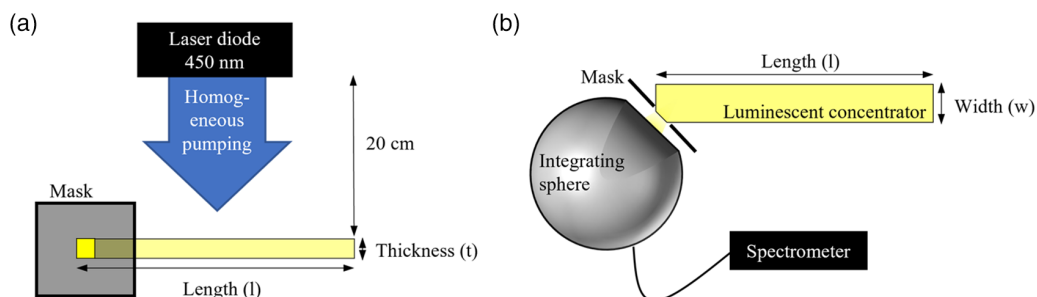


Figure 7. Schematic of: a) a side view and b) top view of the experiment for the edge configuration. For a better understanding, the integrating sphere is represented relatively far from the emitting surface whereas in the real setup the emitting face is in the plane of the integrating sphere aperture.

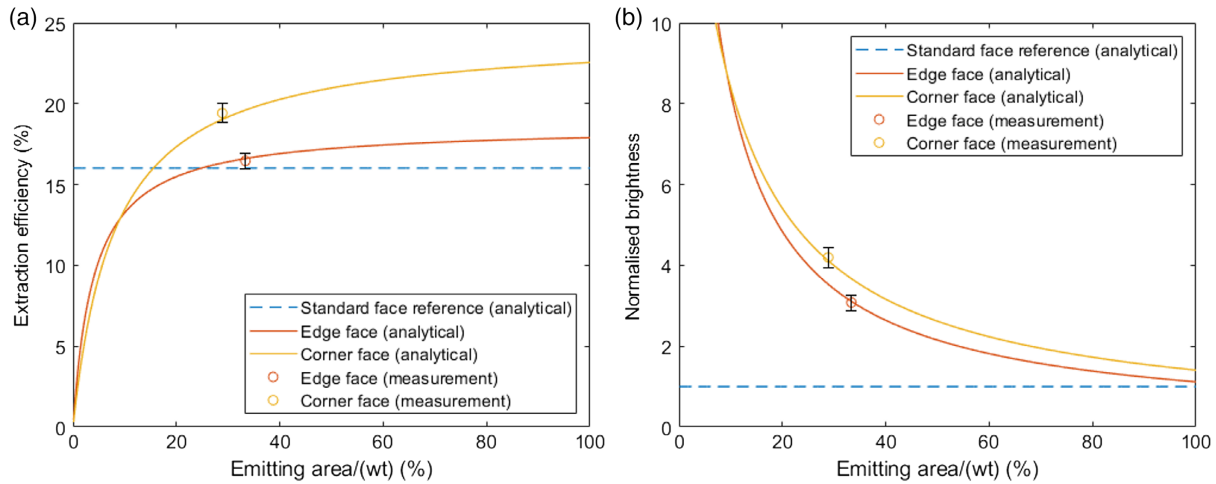


Figure 8. a) Extraction efficiency and b) normalized brightness of the edge and corner face as a function of the emitting area normalized by the standard face emitting area. The curves are plotted for a $22 \times 3 \times 1 \text{ mm}^3$ slab with the propagation losses of Ce:YAG with $3.8 \cdot 10^{-3} \text{ cm}^{-1}$ propagation losses. The experimental values have been determined from the measured ratios to the standard face reference and assuming that the latter is correctly given by the analytically calculated value.

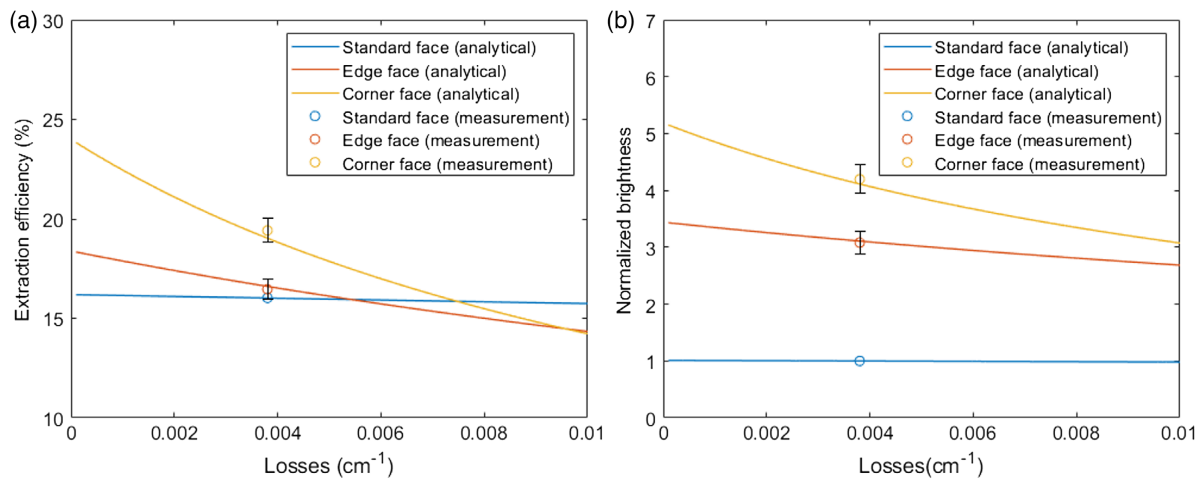


Figure 9. a) Extraction efficiency and b) brightness as a function of the propagation losses for the standard, edge, and corner faces of the Ce:YAG slabs. The curves are plotted for a $22 \times 3 \times 1 \text{ mm}^3$ slab with the propagation losses of Ce:YAG. The sizes of the edge and corner faces are the ones of the experimental samples.

4.4. Influence of the Refractive Index

Figure 10 shows the analytical extraction efficiency and brightness of the emitting face in each configuration as a function of the refractive index. In this section, mirrors have been added on the lateral faces for the edge configuration to explore its potential.

Therefore, four configurations are investigated: 1) the standard face (which includes a mirror on the opposite face), the edge face with: 2) mirrors and 3) without mirrors on the lateral faces, and 4) the corner face (the analytical description of the edge configuration with mirrors is described in the Supporting Information). The best performance is obtained for the edge configuration with mirrors. Experimentally, the light extraction is 1.9 times higher than in the standard configuration. The brightness

is 5.6 times higher. The experimental extraction and brightness obtained for this configuration agree with the theoretical models.

The general shape of the curves can be explained physically. Indeed, the extraction efficiency decreases for the lowest refractive indexes because of the strong overlaps of the escape cones. When mirrors are used on the edge configuration to compensate for the losses of the overlaps, the efficiency drop for low indexes is then far less significant. For high refractive indexes, the extraction efficiency also decreases because of the reduction of the size of the output cone. It can be noticed that among all configurations, the best extraction efficiencies are obtained for $n = 1.36$ with the standard configuration or for edge output face with lateral mirrors. Indeed, for this index value, the size of the escape cone versus the overlapping ratio is optimized. In the index range between 1.5 and 2 (corresponding to typical glass and crystal

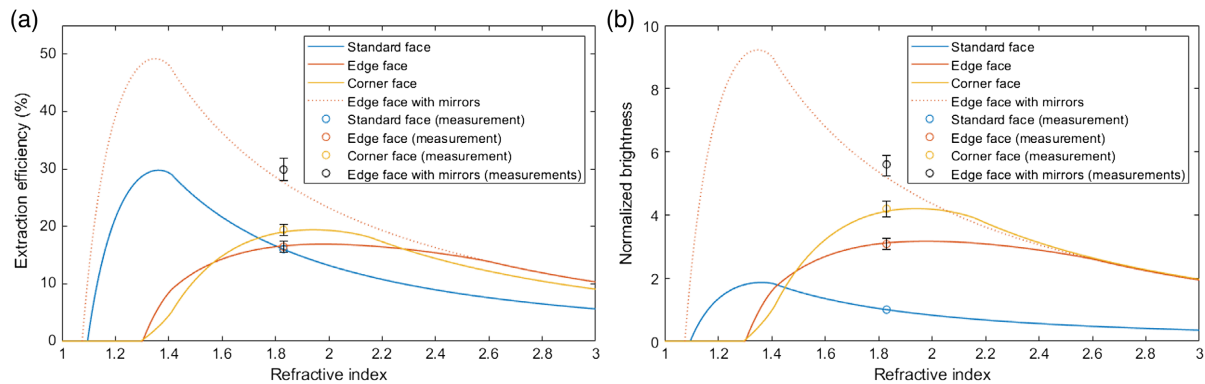


Figure 10. a) Extraction efficiency and b) normalized brightness as a function of the refractive index of the slab for the three configurations (standard face, edge face, and corner face) and the edge face with mirrors on the four lateral faces of the slab. The curves area plotted for $22 \times 3 \times 1 \text{ mm}^3$ slabs with the propagation losses of Ce:YAG and a mirror reflectivity of 99.4%. The sizes of the edge and corner faces are the ones corresponding to the experimental samples.

indices), the extraction efficiencies are globally equivalent (between 15% and 20%) for standard face, edge face, and corner face configurations; only the edge output face with lateral mirrors allows obtaining more than 30% of extraction. In contrast, the brightness obtained with the different configurations is much more spread in favor of the edge output face with lateral mirrors and the corner face configurations.

5. Conclusion

This study presented for the first time a full analytical description of the extraction efficiency of the luminescent slab by an additional face. It demonstrated the interest of an additional face for higher extraction efficiency and higher brightness. An experimental approach performed with Ce:YAG slabs corroborate the analytical description. The additional face has two advantages. The first one was the orientation of the slab, chosen to exploit the symmetry of the structure and multiply the number of cones coupled to the output direction. Two orientations of the additional face have been tested: the edge face and the corner face. At a first glance, the corner face could seem much more attractive since it coupled twice more cones of rays toward the output direction than the edge face. However, its orientation modifies the propagation of the rays such that half of the power is lost by the escape of perturbed rays through the other slab faces. This is the reason why both configurations (edge and corner face) give roughly the same results in terms of brightness, especially for large refractive indices ($n > 2.4$). For lower refractive indices,

the overlap between the output cones and the escape cones of the structure limited the extraction efficiency. As the corner face fully exploited the three dimensions of space, the overlap is then less restrictive. This explained why a corner additional face could be preferable for indices between 1.5 and 2.4. Nevertheless, the edge configuration with mirrors on the lateral faces gave better results since it is insensitive to the overlap with the escape cones on the lateral faces (and also to the large faces providing the index is larger than 1.41). This is the reason why this configuration is preferred. Table 2 gives the benefit of the edge face compared to a standard configuration (having an output on the smallest face of the slab). For many luminescent materials relative to various applications, the additional face provided an improvement in extraction efficiency higher than 1.6 and even close to 2 for large refractive indices.

The second advantage of the additional face was its area, which can be easily controlled and considerably reduced compared to the area of the standard face configuration. Thank to light recycling, the additional face has the potential to increase the brightness by one order of magnitude. The price paid was a decrease of the extraction efficiency imposed by the propagation losses in the structure, reinforced by long travel distances before the rays find the output. Balancing the extraction efficiency and the brightness, we demonstrated experimentally that a $22 \times 3 \times 1 \text{ mm}^3$ Ce:YAG slab with an optimized edge face and covered by mirrors on its lateral faces exhibits an efficiency 1.9 times better and a brightness 5.6 higher than a standard configuration with a Ce:YAG of same dimensions.

Table 2. Performance of the edge face compared to the standard face for commonly used materials (assuming the same dimensions and characteristics as the host-material used in the experiment).

Material	Index	Application	Extraction efficiency of the standard face	Extraction efficiency of the edge face with lateral mirrors	Extraction efficiency of the edge face without lateral mirrors
Dye-doped PMMA	1.49	Luminescent concentrator	25.3%	41.2%	11.8%
Ce:YAG	1.83	Luminescent concentrator/scintillators	16.0%	27.6%	16.5%
BGO	2.16	Scintillators	11.2%	20.0%	16.6%
NV Diamond	2.41	Magnetometry	8.8%	16.1%	15.2%

Therefore, luminescent slabs with an additional face could considerably improve the light collection through standard optics. We believe that this work is a key enabler for better detectors in the scintillation domain, for solid-state magnetometers using NV diamonds, and for new powerful bright sources using LED-pumped concentrators. From this point of view, we have demonstrated an original easy-to-use analytic model validated experimentally to facilitate the design of such geometries for different applications.

6. Experimental Section

Derivation of the overlap between two spherical cones (general case): Let's consider two cones on the unit sphere with a respective half-angle θ_1 and θ_2 (Figure 11a). Here, a general case was derived where θ_1 and θ_2 can have different values. In practice, this corresponds to the cases where the faces are immersed in two media of different refractive index. The apex of the first cone was defined by the O_z axis and the angle between the two cones is γ (the condition for the overlap to exist is $\gamma \leq \theta_1 + \theta_2$). M and N are, respectively, the apex of the first and the second cones. P and Q are the intersection of the two circles of the cones (Figure 11b). The angles φ_1 and φ_2 are, respectively, the apex angle of the spherical triangles defines by the points QMP and PNQ ($\varphi_1 = \widehat{QMP}$, $\varphi_2 = \widehat{PNQ}$). The angles ψ_1 and ψ_2 are, respectively, the base angle of the spherical triangles defines by the points QMP and PNQ ($\psi_1 = \widehat{MPQ}$ and $\psi_2 = \widehat{NQP}$).

According to Archimedes' hat box theorem, the area of the spherical triangles QMP and PNQ are, respectively, $\Omega_{QMP} = \varphi_1(1 - \cos\theta_1)$ and $\Omega_{PNQ} = \varphi_2(1 - \cos\theta_2)$. The area of the spherical quadrilateral is $\Omega_{MNPQ} = \varphi_1 + \varphi_2 + 2(\psi_1 + \psi_2) - 2\pi$ (from the general formula of the area of an N-sided spherical polygon^[41]). Then, the area of the overlap between the cones is

$$\Omega_{\text{overlap}} = \Omega_{QMP} + \Omega_{PNQ} - \Omega_{MNPQ} = 2\pi - 2(\psi_1 + \psi_2) - \varphi_1(1 - \cos\theta_1) - \varphi_2(1 - \cos\theta_2) \quad (21)$$

Now, φ_1 , φ_2 , ψ_1 , and ψ_2 have to be expressed with θ_1 , θ_2 , and γ to know the area of the overlap with the TIR condition and the relative inclination of the faces. The angle \widehat{CAB} defined by three points A, B, and C on the unit sphere centered on O can be calculated via the scalar product of two vectors, respectively, orthogonal to the plans OAB and OAC (a vector orthogonal to the plan OAB being the normalized cross product between the vectors \vec{OA} and $\vec{O}(B - \vec{A})$).

The coordinates of the four points M, N, P, and Q can be expressed with θ_1 , θ_2 , and γ

$$M = \begin{pmatrix} 0 \\ 0 \\ 1 \end{pmatrix}; \quad N = \begin{pmatrix} \sin\gamma \\ 0 \\ \cos\gamma \end{pmatrix}; \quad P = \begin{pmatrix} a \\ -b \\ \cos\theta_1 \end{pmatrix}; \quad Q = \begin{pmatrix} a \\ b \\ \cos\theta_1 \end{pmatrix} \quad (22)$$

with

$$a = \frac{\cos\theta_2 - \cos\theta_1 \cos\gamma}{\sin\gamma} \quad (23)$$

and

$$b = \sqrt{\sin^2\theta_1 - a^2} \quad (24)$$

Applying the method described to calculate the angle \widehat{CAB} for three points on the unit sphere to $\varphi_1 = \widehat{QMP}$, $\varphi_2 = \widehat{PNQ}$, $\psi_1 = \widehat{MPQ}$, and $\psi_2 = \widehat{NQP}$, the four angles can be expressed only with θ_1 , θ_2 , and γ as below.

$$\varphi_1 = \widehat{QMP} = \arccos \left[\frac{a^2 - b^2}{a^2 + b^2} \right] \quad (25)$$

$$\varphi_2 = \widehat{PNQ} = \arccos \left[\frac{(a \cos\gamma - \sin\theta \cos\theta_1)^2 - b^2}{(a \cos\gamma - \sin\theta \cos\theta_1)^2 + b^2} \right] \quad (26)$$

$$\psi_1 = \widehat{MPQ} = \arccos \left[\frac{b \cos\theta_1}{\sqrt{(a^2 + b^2)(a^2 + \cos^2\theta_1)}} \right] \quad (27)$$

$$\psi_2 = \widehat{NQP} = \arccos \left[\frac{b \cos\theta_1 \cos\gamma + ba \sin\gamma}{\sqrt{((a \cos\gamma - \sin\gamma \cos\theta_1)^2 + b^2)(a^2 + \cos^2\theta_1)}} \right] \quad (28)$$

The combination of Equation (21), (25)–(28), allows to express Ω_{overlap} only with the TIR conditions and the relative inclination of the faces (θ_1 , θ_2 , and γ).

In the scope of this article, all the faces of the slab are in air which implies that $\theta_1 = \theta_2 = \theta_{\text{TIR}}$. Then, when the value of the overlap between two cones is used in an equation it is referred to by $\Omega_{\text{overlap}, \gamma}$.

Light is isotropically emitted inside the luminescent rectangular slab (i.e., emitted in 4π steradians corresponding to the surface of the unit sphere). Then, the ratio of trapped light (or trapping ratio) is calculated by the subtraction of the six escape cones (one cone per face). The sphere is fully covered by escape cones when the total internal reflection angle is

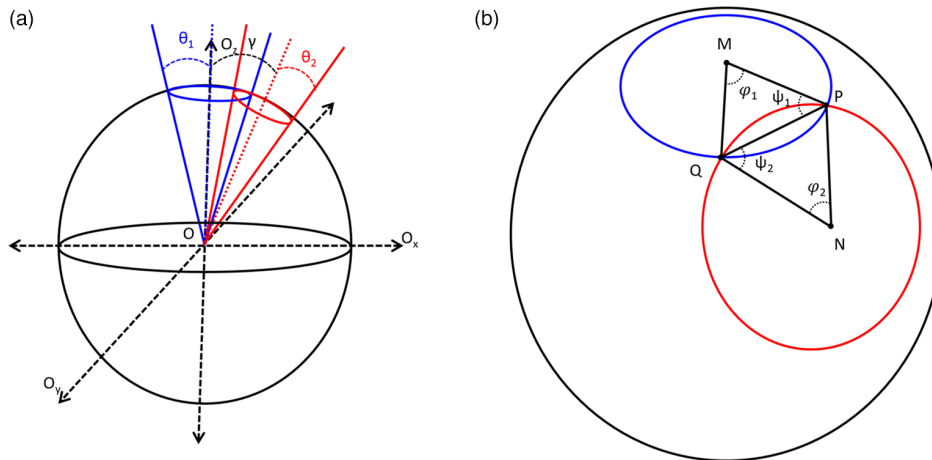


Figure 11. Schematics of the two cones on the sphere and definition of the angles: a) general view, b) focus on the overlap.

equal to the angle of the vector of the diagonal of the slab ($\theta_{\text{TIR}} = \text{asin}(\sqrt{2/3}) = 55^\circ$). This condition corresponds to $n = 1.22$ in terms of refractive index. Thus, there are no trapped rays for $n \leq 1.22$. When the escape cones do not overlap, which corresponds to the cases $\theta_{\text{TIR}} \leq \text{asin}(1/\sqrt{2}) = 45^\circ$ (i.e., $n \geq 1.41$), six escape cones are subtracted to 4π . When $1.22 \leq n \leq 1.41$, the overlaps of the cones must be considered (12 overlaps of value $\Omega_{\text{overlap},90^\circ}$).

The trapping ratio (Equation (29)) is plotted versus the refractive index of the rectangular slab in **Figure 12**.

$$\eta_{\text{trapped}} = \begin{cases} 4\pi - 6\Omega_{\text{escape}}, & \text{if } n \geq 1.41 \\ \frac{4\pi}{4\pi - 6\Omega_{\text{escape}} + 12\Omega_{\text{overlap},90^\circ}}, & \text{if } 1.22 \leq n \leq 1.41 \\ 0, & \text{if } n \leq 1.22 \end{cases} \quad (29)$$

Derivation of the Overlaps in the Standard Rectangular Slab Case: In the case of standard rectangular slabs without any additional faces, there are six escape cones each of them corresponding to a face of the slab. Each spherical cone is next to four cones with a relative angle of 90° (Figure 1). Hence, the overlap between two cones is $\Omega_{\text{overlap},90^\circ}$. The expression of the overlapping ratio ($\eta_{\text{overlap},s}$) changes with the refractive index (Figure S3, Supporting Information, gives a schematics of the overlaps for the different conditions).

If $\theta_{\text{TIR}} \leq 45^\circ$ (i.e., $n \geq 1.41$), there are no overlaps. If $\theta_{\text{TIR}} \geq 45^\circ$ (i.e., $n \leq 1.41$), 2 cases must be distinguished. First, if $\theta_{\text{TIR}} \geq 55^\circ$ (i.e., $n \leq 1.22$), the overlapping ratio is close to 1 but second-order overlaps appear which complicates calculations. As the case of a luminescent slab of the refractive index of 1.22 or less is far from the considerations, the trapping ratio is approximated by 1 in this case. If $45^\circ \leq \theta_{\text{TIR}} \leq 55^\circ$ (i.e., $1.22 \leq n \leq 1.41$) one overlap from each of the four surrounding cones has to be considered. The overlapping ratio (Equation (30)) is plotted in Figure 4.

$$\eta_{\text{overlap},s} = \begin{cases} 0, & \text{if } n \geq 1.41 \\ \frac{4\Omega_{\text{overlap},90^\circ}}{\Omega_{\text{escape}}}, & \text{if } 1.22 \leq n \leq 1.41 \\ \sim 1, & \text{if } n \leq 1.22 \end{cases} \quad (30)$$

Derivation of the Overlaps in the Case of an Edge Face: In the case described in Section 3.1, an additional edge face is added to the rectangular slab with angles ($\alpha = 45^\circ$ and $\beta = 0^\circ$). The escape cone is

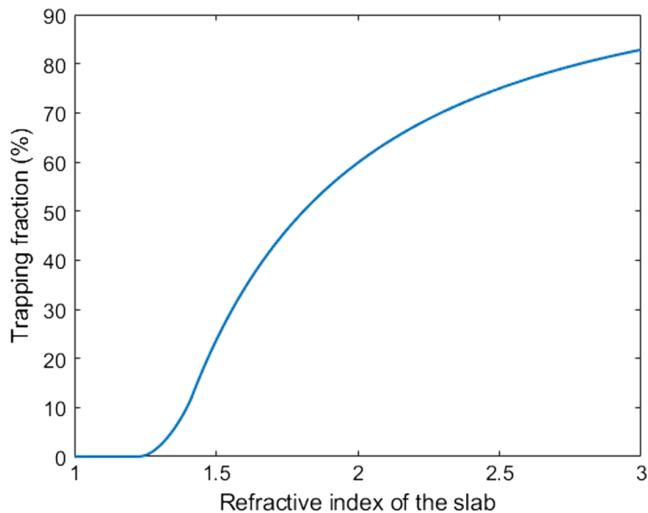


Figure 12. Trapped rays (in percent) inside a luminescent rectangular slab in air as a function of its refractive index.

surrounded by two pairs of cones with different relative angles (Figure 4). First, two cones with a relative angle of 45° which overlaps if $\theta_{\text{TIR}} \geq \text{sin}(\pi/8) = 22.5^\circ$ (i.e., $n \leq 2.61$) with a value of $\Omega_{\text{overlap},45^\circ}$. Second, two cones with a relative angle of 90° which overlaps if $\theta_{\text{TIR}} \geq 45^\circ$ (i.e., $n \leq 1.41$) with a value of $\Omega_{\text{overlap},90^\circ}$. When $n \leq 1.41$, the overlap between the two cones at 45° which are also distant from 90° must be considered (see Figure S4, Supporting Information). The overlapping ratio (Equation (31)) is plotted in Figure 4.

$$\eta_{\text{overlap},e} = \begin{cases} 0, & \text{if } n \geq 2.61 \\ \frac{2\Omega_{\text{overlap},45^\circ}}{\Omega_{\text{escape}}}, & \text{if } 1.41 \leq n \leq 2.61 \\ \frac{2\Omega_{\text{overlap},45^\circ} + \Omega_{\text{overlap},90^\circ}}{\Omega_{\text{escape}}}, & \text{if } n \leq 1.41 \end{cases} \quad (31)$$

Derivation of the Overlaps in the Case of a "Corner Face": In the case described in Section 3.2, an additional corner face is added to the rectangular slab with angles ($\alpha = 45^\circ$ and $\beta = 35^\circ$). The escape cone is surrounded by three cones with a relative angle of $\text{asin}(\sqrt{2/3}) = 55^\circ$ (see Figure 6 and S5, Supporting Information). The overlap starts for $\theta_{\text{TIR}} \geq \text{asin}(1/\sqrt{6}) = 27.5^\circ$ (i.e., $n \leq 2.16$) and its value is $\Omega_{\text{overlap},45^\circ}$. When $n \leq 1.41$, the three cones at 55° start to overlap each other: the value of $\eta_{\text{overlap},c}$ can be approximated. When $\theta_{\text{TIR}} \geq \text{asin}(\sqrt{2/3}) = 55^\circ$ the additional face is totally overlapped. $\eta_{\text{overlap},c}$ is plotted in Figure 4.

$$\eta_{\text{overlap},c} = \begin{cases} 0, & \text{if } n \geq 2.16 \\ \frac{3\Omega_{\text{overlap},55^\circ}}{\Omega_{\text{escape}}}, & \text{if } 1.41 \leq n \leq 2.16 \\ \frac{3\Omega_{\text{overlap},55^\circ} - \frac{3}{2}\Omega_{\text{overlap},90^\circ}}{\Omega_{\text{escape}}}, & \text{if } 1.22 \leq n \leq 1.41 \\ 1, & \text{if } n \leq 1.22 \end{cases} \quad (32)$$

The power related to the rays emitted in the (1,1,1), (1,1,-1), (1,-1,-1), and (1,-1,1) escape cones is

$$P_{(1,1,1)} = P_{(1,1,-1)} = P_{(1,-1,-1)} = P_{(1,-1,1)} \\ = \frac{\phi_e n_i w t}{2\sqrt{3}ad} (1 - \cos \theta_{\text{RTI}}) (1 - e^{-\sqrt{3}ad}) \quad (33)$$

The first time that light crosses the plane of the corner face, it exits by the face with a probability of $3t/(8w)$.

$$P_{(1,1,1),1} = \frac{3tT}{8w} P_{(1,1,1)} \quad (34)$$

A part of the light did not encounter the exit face and is recycled inside the rectangular slab. It propagates a distance of $2\sqrt{3}d$ before having another chance to be extracted. The output power after the second time that light crosses the plane of the corner face is

$$P_{(1,1,1),2} = \frac{3tT}{8w} e^{-2\sqrt{3}ad} \left(1 - \frac{3tT}{8w}\right) P_{(1,1,1)} \quad (35)$$

The total output power from this escape cone is

$$P_{(1,1,1),\text{tot}} = \sum_{k=0}^{\infty} P_{(1,1,1),k} = \frac{3tT}{8w} P_{(1,1,1,0)} \frac{1}{1 - e^{-2\sqrt{3}ad} \left(1 - \frac{3tT}{8w}\right)} \quad (36)$$

The same method allows to find the contribution of the rays emitted in the (-1,1,1), (-1,1,-1), (-1,-1,-1), and (-1,-1,1) escape cones with

$$P_{(-1,1,1)} = P_{(-1,1,-1)} = P_{(-1,-1,-1)} = P_{(-1,-1,1)} \\ = \frac{\phi_e n_i \omega l t}{2\sqrt{3}\alpha d} (1 - \cos \theta_{RTI}) e^{-2\sqrt{3}\alpha d} (e^{\sqrt{3}\alpha d} - 1) \quad (37)$$

By summing the contribution of each spherical cone and taking into account the overlapping ratio, the power emitted by the edge face is

$$P_c = (1 - \eta_{\text{overlap},c}) \sum P_{(\pm 1, \pm 1, \pm 1), \text{tot}} \quad (38)$$

Equation (38) can be expressed literally by

$$P_c = (1 - \eta_{\text{overlap},c}) \\ (1 - \eta_d) \frac{\sqrt{3} t}{2} \frac{\phi_e n_i \omega l t}{w} \frac{(1 - \cos \theta_{RTI}) (1 + e^{-\sqrt{3}\alpha d}) (1 - e^{-\sqrt{3}\alpha d}) T}{2\alpha d} \frac{1 - e^{-2\sqrt{3}\alpha d} (1 - \frac{3T}{8w})}{1 - e^{-2\sqrt{3}\alpha d} (1 - \frac{3T}{8w})} \quad (39)$$

Supporting Information

Supporting Information is available from the Wiley Online Library or from the author.

Acknowledgements

Centre National de la Recherche Scientifique (CNRS pre-maturation LEDsGO project); Agence Nationale de la Recherche (ANR-10-LABX-0039-PALM).

Conflict of Interest

The authors declare no conflict of interest.

Data Availability Statement

The data that support the findings of this study are available from the corresponding author upon reasonable request.

Keywords

brightness, light guide, luminescent concentrator, luminescent materials, scintillators

Received: November 26, 2021

Revised: February 11, 2022

Published online:

-
- [1] A. I. Zhmakin, *Phys. Rep.* **2011**, 498, 189.
 [2] E. Khaidarov, Z. Liu, R. Paniagua-Domínguez, S. T. Ha, V. Valuckas, X. Liang, Y. Akimov, P. Bai, C. E. Png, H. V. Demir, A. I. Kuznetsov, *Laser Photonics Rev.* **2019**, 14, 1900235.
 [3] W. A. Shurcliff, R. Clark Jones, *J. Opt. Soc. Am.* **1949**, 39, 912.
 [4] G. Keil, *Nucl. Instrum. Methods* **1970**, 87, 111.
 [5] G. Hull, S. Du, T. Niedermayr, S. Payne, N. Cherepy, A. Drobshoff, L. Fabris, *Nucl. Instrum. Methods Phys. Res. A* **2008**, 588, 384.
 [6] S. R. Cherry, Y. Shao, M. P. Tornai, S. Siegel, A. R. Ricci, M. E. Phelps, *IEEE Trans. on Nucl. Sci.* **1995**, 42, 1058.
 [7] K. Katrunov, V. Ryzhikov, V. Gavriilyuk, S. Naydenov, O. Lysetska, V. Litichevskiy, *Nucl. Instrum. Methods Phys. Res. A* **2013**, 712, 126.
 [8] F. A. Danevich, V. V. Kobychiev, R. V. Kobychiev, H. Kraus, V. B. Mikhailik, V. M. Mokina, I. M. Solsky, *Nucl. Instrum. Methods Phys. Res. B* **2014**, 336, 26.
 [9] C. Carrier, R. Lecomte, *Nucl. Instrum. Methods Phys. Res. A* **1990**, 294, 355.
 [10] C. M. Ankenbrandt, E. M. Lent, *Rev. Sci. Instrum.* **1963**, 34, 647.
 [11] E. Yablonovitch, *J. Opt. Soc. Am.* **1980**, 70, 1362.
 [12] W. H. Weber, J. Lambe, *Appl. Opt.* **1976**, 15, 2299.
 [13] F. Meinardi, A. Colombo, K. A. Velizhanin, R. Simonutti, M. Lorenzon, L. Beverina, R. Viswanatha, V. I. Klimov, S. Brovelli, *Nat. Photonics* **2014**, 8, 392.
 [14] F. Meinardi, H. McDaniel, F. Carulli, A. Colombo, K. A. Velizhanin, N. S. Makarov, R. Simonutti, V. I. Klimov, S. Brovelli, *Nat. Nanotechnol.* **2015**, 10, 878.
 [15] F. Meinardi, S. Ehrenberg, L. Dharmo, F. Carulli, M. Mauri, F. Bruni, R. Simonutti, U. Kortshagen, S. Brovelli, *Nat. Photonics* **2017**, 11, 177.
 [16] J. Sathian, N. M. Alford, M. Oxborrow, *Proc. SPIE Photonics West (OPTO)* **2015**, 9359, 9359.
 [17] J. Sathian, J. D. Breeze, B. Richards, N. M. Alford, M. Oxborrow, *Opt. Express* **2017**, 25, 13714.
 [18] D. K. G. de Boer, D. Bruls, H. Jagt, *Opt. Express* **2016**, 24, A1069.
 [19] C. Hoelen, D. K. G. de Boer, D. Bruls, J. van der Eyden, R. Koole, Y. Li, M. Mirsadeghi, V. Vanbroekhoven, J.-J. Van den Bergh, P. Van de Voorde, *Proc. SPIE* **2016**, 9768, 9768.
 [20] D. K. G. de Boer, D. Bruls, H. Jagt, C. Hoelen, *Proc. SPIE* **2017**, 10378, 103780M.
 [21] D. K. G. de Boer, L. Haenen, *J. Eur. Opt. Soc.* **2019**, 15, 8.
 [22] P. Pichon, J.-P. Blanchot, F. Balembois, P. Georges, *Opt. Express* **2018**, 26, 9353.
 [23] A. Barbet, A. Paul, T. Gallinelli, F. Balembois, J.-P. Blanchot, S. Forget, S. Chénais, F. Druon, P. Georges, *Optica* **2016**, 3, 465.
 [24] P. Pichon, A. Barbet, J.-P. Blanchot, F. Druon, F. Balembois, P. Georges, *Optica* **2018**, 5, 1236.
 [25] P. Pichon, A. Barbet, F. Druon, J.-P. Blanchot, F. Balembois, P. Georges, *Opt. Lett.* **2017**, 42, 4191.
 [26] H. Taleb, P. Pichon, F. Druon, F. Balembois, P. Georges, *Opt. Lett.* **2021**, 46, 2421.
 [27] J. Walker, *Rep. Prog. Phys.* **1979**, 42, 1605.
 [28] S. Pezzagna, D. Rogalla, D. Wildanger, J. Meijer, A. Zaitsev, *New J. Phys.* **2011**, 13, 35024.
 [29] A. Kuwahata, T. Kitaizumi, K. Saichi, T. Sato, R. Igarashi, T. Ohshima, Y. Masuyama, T. Iwasaki, M. Hatano, F. Jelezko, M. Kusakabe, T. Yatsui, M. Sekino, *Sci. Rep.* **2020**, 10, 1.
 [30] T. Wolf, P. Neumann, K. Nakamura, H. Sumiya, T. Ohshima, J. Isoya, J. Wrachtrup, *Phys. Rev. X* **2015**, 5, 041001.
 [31] L. Xu, H. Yuan, N. Zhang, J. Zhang, G. Bian, P. Fan, M. Li, C. Zhang, Y. Zhai, J. Fang, *Opt. Express* **2019**, 27, 10787.
 [32] A. Gruber, A. Drabenstedt, C. Tietz, L. Fleury, J. Wrachtrup, C. von Borczyskowski, *Science* **1997**, 276, 2012.
 [33] P. Pichon, F. Balembois, F. Druon, P. Georges, *Opt. Express* **2021**, 29, 6915.
 [34] T. Gallinelli, A. Barbet, F. Druon, F. Balembois, P. Georges, T. Billeton, S. Chenais, S. Forget, *Opt. Express* **2019**, 27, 11830.
 [35] S. Roelandt, Y. Meuret, D. K. G. de Boer, D. Bruls, P. Van De Voorde, H. Thienpont, *Opt. Eng.* **2015**, 54, 055101.
 [36] R. J. Epstein, F. M. Mendoza, Y. K. Kato, D. D. Awschaldom, *Nat. Phys.* **2005**, 1, 94.
 [37] M. Dréau, L. Lesik, P. Rondin, O. Spinicelli, O. Arcizet, J.-F. Roch, V. Jacques, *Phys. Rev. B* **2011**, 84, 195204.

- [38] R. Brouri, A. Beveratos, J.-P. Poizat, P. Grangier, *Opt. Lett.* **2000**, 25, 1294.
- [39] P. Siyushev, F. Kaiser, V. Jacques, I. Gerhardt, S. Bischof, H. Fedder, J. Dodson, M. Markham, D. Twitchen, F. Jelezko, J. Wrachtrup, *Appl. Phys. Lett.* **2010**, 97, 241902.
- [40] M. Nourry-Martin, P. Pichon, F. Druon, S. Darbon, F. Balembois, P. Georges, *Opt. Express* **2021**, 29, 25302.
- [41] I. Todhunter, *Spherical Trigonometry* 5th ed., MacMillan, London, **1886**.